

Swarm-optimized Adaptive Augmentation of Missile Autopilot

Alexander Dorsey*, Parham Oveissi†, Jeffrey D. Barton‡, Ankit Goel§

This paper considers the problem of optimizing a missile autopilot. In particular, the paper investigates the application of an online learning technique to learn and optimize the gains of a three-loop topology autopilot for a planar missile modeled with nonlinear dynamics and nonlinear aerodynamics forces and moments. The classical autopilot for a missile is based on a three-loop topology, where each loop consists of tunable proportional gains. An adaptive three-loop autopilot is constructed by augmenting the classical autopilot's fixed-gain controllers with a learning-based controller, which is recursively optimized using retrospective cost optimization. Numerical simulations show that online learning improves the tracking performance of the classical autopilot in both nominal and off-nominal interception scenarios.

I. Introduction

The design of autopilots for missiles is a challenging control problem due to several factors, including nonlinear dynamics, nonminimum phase behavior due to nose-mounted gyro sensor and tail-fin actuation, and uncertain aerodynamic loading. Furthermore, in a typical mission, a missile undergoes a range of Mach numbers and aggressive maneuvers, which results in strongly varying aerodynamic loading. Model-based control of missiles is thus impractical. Instead, a common classical missile autopilot is based on a three-loop topology that uses the IMU data, including the acceleration and angular velocity measurements, with flight-scheduled gains. The gain-scheduled controller consists of gains scheduled to several operating conditions. However, designing the controller gains for each operating condition is expensive and time-consuming.

Several nonlinear adaptive control techniques have been investigated for missile autopilot design. Model-based nonlinear control techniques such as adaptive backstepping is explored in [1], \mathcal{L}_1 control is explored in [2], MRAC is explored in [3], input-output linearization is explored in [4, 5], and Lyapunov-based approaches are explored in [6, 7]. In this paper, we consider the retrospective cost adaptive control (RCAC) to recursively optimize the gains of a classical three-loop autopilot. RCAC has been previously investigated for the missile control application. In particular, an auto-regressive-moving-average adaptive control law was used to generate pitch rate commands in [8], whereas RCAC was used to improve the missile's ability to intercept a target under sensor failures in [9]. However, this paper investigates the ability of RCAC to tune the gains of the three-loop autopilot. In particular, we augment the fixed-gain controllers in the three-loop autopilot with adaptive controllers in parallel. This architecture allows RCAC to both improve the autopilot's tracking performance as well as automatically tune the gains of the autopilot from measured data instead of models.

The paper is organized as follows. Section II briefly reviews the nonlinear dynamics of a missile and the classical three-loop autopilot topology. Section III presents the adaptive augmentation of the three-loop autopilot. Three scenarios are presented in Section IV to investigate the performance of the adaptive autopilot in nominal and off-nominal conditions. Finally, the paper concludes with a summary in Section V.

II. Missile Dynamics and Control

This section briefly reviews the equations of motion of a missile and the classical three-loop autopilot.

A. Longitudinal Dynamics

Let F_A be an inertial frame and let F_B be a frame fixed to the missile body as shown in Figure 1. The frame F_B is obtained by rotating it about \hat{j}_A by the *pitch angle* θ ,

and thus $\vec{\omega}_{B/A} = \dot{\theta}\hat{j}_B$. Let c denote the center of mass of the missile and let w denote a point with zero inertial acceleration. Let F_C be a frame such that $\hat{i}_C = \hat{v}_{c/w/A}$ and $\hat{j}_C = \hat{j}_B$, where $\hat{v}_{c/w/A}$ is the unit vector along the velocity

*Undergraduate Student, Department of Mechanical Engineering, 1000 Hilltop Circle, Baltimore, MD 21250.

†Graduate Student, Department of Mechanical Engineering, 1000 Hilltop Circle, Baltimore, MD 21250.

‡Principal Staff, Johns Hopkins University Applied Physics Laboratory, Laurel, MD, 20723.

§Assistant Professor, Department of Mechanical Engineering, 1000 Hilltop Circle, Baltimore, MD 21250.

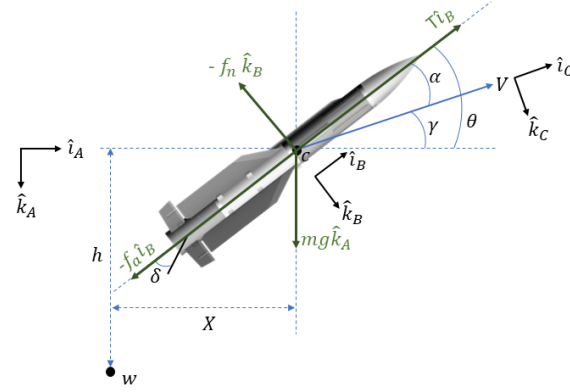


Fig. 1 Free body diagram of a missile.

$\vec{v}_{c/w/A}$ of the missile. Therefore, $\vec{v}_{c/w/A} = V\hat{i}_C$, where V is the magnitude of the missile velocity. Note that the frame F_C is obtained by rotating it about \hat{j}_A by the *flight path angle* γ .

The *angle of attack* is thus $\alpha \triangleq \theta - \gamma$.

The equations of motion of a missile are

$$\dot{M} = \frac{T}{ma} \cos(\alpha) - \frac{g}{a} \sin(\gamma) - \frac{\rho a M^2 S}{2m} [C_N \sin(\alpha) + C_A \cos(\alpha)], \quad (1)$$

$$\dot{\gamma} = \frac{T}{maM} \sin(\alpha) - \frac{g}{aM} \cos(\gamma) + \frac{\rho a M S}{2m} [C_N \cos(\alpha) - C_A \sin(\alpha)], \quad (2)$$

$$\dot{\theta} = q, \quad (3)$$

$$\dot{q} = \frac{\rho a^2 M^2 S d}{2I_y} C_M, \quad (4)$$

$$\dot{h} = Ma \sin(\gamma), \quad (5)$$

$$\dot{X} = Ma \cos(\gamma), \quad (6)$$

where m is the mass of the missile, a is the speed of sound, M is the Mach number, T is the thrust applied to the missile along \hat{i}_B , I_y is the moment of inertia, q is the pitch rate, h is the altitude, and X is the downrange. The derivation of the equations of motion (1)-(6) and the vehicle parameters used in this study are detailed in Appendix A. The aerodynamic coefficients C_N , C_A , and C_M are nonlinear functions of the angle of attack α , fin deflection angle δ , and the pitch rate q , as shown in (20)-(22).

B. Three-loop Autopilot

This section briefly reviews the three-loop autopilot. Several multi-loop autopilot topologies for normal-acceleration tracking are described in more detail in [10]. The control architecture for normal acceleration tracking is shown in Figure 2. In practice, the normal acceleration reference $a_{z,\text{ref}}$ is given by the guidance law. The three-loop autopilot uses the reference normal acceleration and the measurements of the normal acceleration and the pitch rate to compute the fin deflection command u .

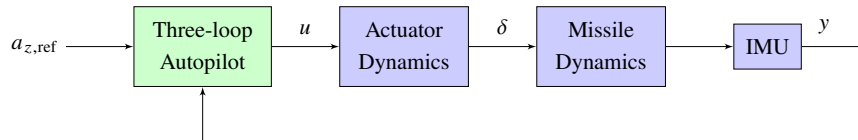


Fig. 2 Control architecture to track normal acceleration commands.

In particular, the control signal u generated by the three-loop autopilot is

$$u = K_q q + \int (K_\theta q + K_a(a_{z,\text{ref}} - K_{a_z} a_z)) dt, \quad (7)$$

where K_q , K_θ , K_a , and K_{a_z} are the tunable proportional gains. In this work, as considered in [10], we set $K_q = 0.464$, $K_\theta = 15.62474$, $K_a = 0.2446459$, and $K_{a_z} = 0.9278$, $a_{z,\text{ref}}$ is the normal acceleration command, a_z is the sensed acceleration at the IMU given by

$$a_z \triangleq a_{z,\text{CG}} - \dot{q} d_{\text{IMU}}, \quad (8)$$

where $d_{\text{IMU}} = 0.5$ m is the distance from the center of gravity to the IMU, and the gravity-corrected normal acceleration of the center of gravity $a_{z,\text{CG}}$ is

$$a_{z,\text{CG}} = \frac{\rho a^2 M^2 S}{2m} C_N. \quad (9)$$

The IMU provides the output vector y that contains the measurements of the normal acceleration a_z and pitch rate q . The implementation of the control law (7) is shown in Figure 3. In the rest of the paper, the three-loop autopilot with fixed gains is denoted by F-TLA.

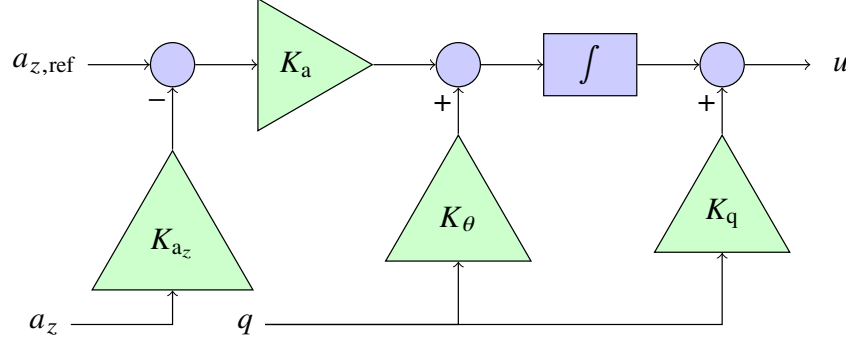


Fig. 3 Classical three loop controller topology [10].

III. Adaptive TLA

In the adaptive augmentation, shown in Figure 4, the input signal computed by the three-loop autopilot is modified as

$$u(t) = u_{\text{TLA}}(t) + u_a(t), \quad (10)$$

where $u_{\text{TLA}}(t)$ is the control signal computed using (7) and $u_a(t)$ is the control signal computed by the adaptive controller. In particular, the control signal $u_a(t)$ is computed by the RCAC algorithm. Since RCAC is a discrete-time algorithm that updates the control signal at a fixed timestep, the control $u_a(t)$ in between the control updates is held constant. Letting T_s denote the timestep, for $t \in (kT_s, (k+1)T_s)$, the control $u_a(t)$ is thus given by

$$u_a(t) = u_k, \quad (11)$$

where k is the iteration number and u_k is the control signal computed by RCAC. In particular, an adaptive dense structured controller, described in [11], is chosen so that the regressor matrix is given by

$$\phi_k = \begin{bmatrix} u_{k-1} & \cdots & u_{k-n_c} & z_{k-1} & \cdots & z_{k-n_c} \gamma_k \end{bmatrix}, \quad (12)$$

where $z_k \triangleq a_{z,\text{ref}} - a_z$, $\gamma_k \triangleq \sum_{i=1}^k z_i$ is the accumulated error, and the adaptive controller gain $\theta_k \in \mathbb{R}^{2n_c+1}$ is updated by retrospective cost optimization. The adaptive control signal u_k is thus an adaptive weighting of the regressor matrix,

in the form of $u_k = \Phi_k \theta_k$. The adaptive weight θ_k is determined at each time step k by minimizing the retrospective cost function

$$J(k) \triangleq \sum_{i=1}^k \lambda^{k-i} [\hat{z}_i^T R_z \hat{z}_i + (\phi_i \hat{\theta})^T R_u (\phi_i \hat{\theta})] + \lambda^k (\hat{\theta} - \theta_0)^T R_\theta (\hat{\theta} - \theta_0), \quad (13)$$

where $\hat{z}_i \triangleq z_i + \phi_{f,i} \hat{\theta} - u_{f,i}$ is the retrospective performance, $\phi_{f,i} \triangleq G_f(\mathbf{q}) \phi_i$ and $u_{f,i} \triangleq G_f(\mathbf{q}) u_i$ are the filtered regressor and the input, \mathbf{q} is the forward-shift operator, λ is a forgetting factor, R_z , R_u , and R_θ are hyperparameters, and G_f is a filter. The RCAC algorithm to compute u_k is described in [12–14].

As shown in [15], the cost function that is retrospectively minimized in RCAC includes a filter, G_f , which should consist of any nonminimum phase zeros of the system. In this work, we update the filter G_f with the real nonminimum phase zeros of the linearized missile dynamics (1)–(6), computed at the current state. Thus, the filter G_f is time varying and is updated at every step. In the rest of the paper, the three-loop autopilot with the adaptive augmentation is denoted by A-TLA.

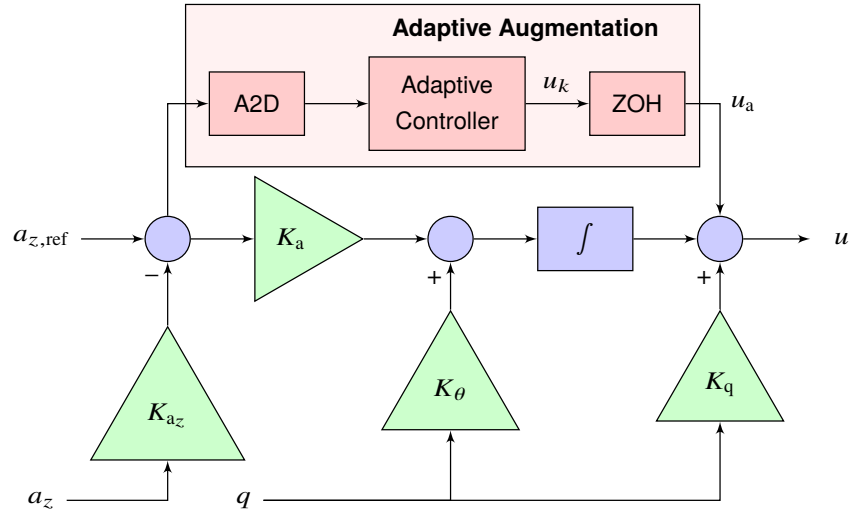


Fig. 4 Adaptive three loop controller topology.

IV. Numerical Simulation

This section investigates the performance improvements with the adaptive augmentation of the TLA. In particular, the performance of the A-TLA is investigated in the case of an arbitrary normal acceleration command and an interception mission scenario, described in Appendix B. The missile dynamics and the TLA described in previous sections are simulated with Matlab's ode45 routine. In all scenarios considered in this paper, the initial Mach number of the missile is 2.5, the initial flight path angle is 45 degrees, the initial pitch angle is 45 degrees, the initial pitch rate is 0 rad/s, the initial altitude is 3,500 m, a constant thrust of 3800 newtons, and the fin deflection angle and its rate are 0 degrees and 0 rad/s, respectively.

A. RCAC Hyperparameter Optimization

The RCAC hyperparameter R_z is held constant at unity, while R_u and R_θ are numerically optimized using a *particle swarm optimization* (PSO) framework. In a PSO, the parameter vector to optimize is treated as a particle with a position and velocity. A swarm of particles are evaluated and each particle's motion is influenced by the best local and global parameters previously found. The objective of PSO is thus to find the set of parameters that minimize a cost function. The cost function used to tune the RCAC hyperparameters in the PSO framework is

$$J_{\text{PSO}} = \frac{1}{N} \sum_{i=1}^N \frac{2}{g} |z_i| + 0.2 \max(|\dot{q}_i| - \dot{q}_{\max}, 0), \quad (14)$$

where $\dot{q}_{\max} = 3$ degrees/s², where N is the length of the simulation, and the data z_i and u_i are generated by the closed-loop response to the command $a_{z,\text{ref}} = 0.5g - 8g\text{sign}(\sin(0.3t))$.

The controller optimized by RCAC is a 4th-order ARMA controller with a built-in integrator. Various parameterizations that can be used in the RCAC framework are described in [16]. Note that, in our preliminary work, the cost function is chosen by trial and error. In the particle swarm, R_u is restricted between 0 and 20 and R_θ is restricted between 10^0 and 10^{15} . The RCAC hyperparameters after swarm optimization are $(R_u, R_\theta) = (0.25427, 10^{14.398})$. In all numerical experiments described next in the paper, the RCAC hyperparameters are fixed.

Next, the performance improvements due to the adaptive augmentation are investigated. The acceleration reference is a constant step of magnitude $10g$. To demonstrate the performance recovery with the adaptive augmentation, we manually degrade the F-TLA by scaling all of its gains by $\alpha_{\text{TLA}} \in \mathbb{R}$. Figure 5 shows the closed-loop step response with the F-TLA and the A-TLA for various scaling factor values α_{TLA} . Note that the performance of the F-TLA and the A-TLA is similar in the case where $\alpha_{\text{TLA}} = 1$. On the other hand, the degraded F-TLA's step response performance degrades, as expected. However, the A-TLA performs similarly for a wide range of α_{TLA} , thus demonstrating the performance improvements due to the adaptive augmentation.

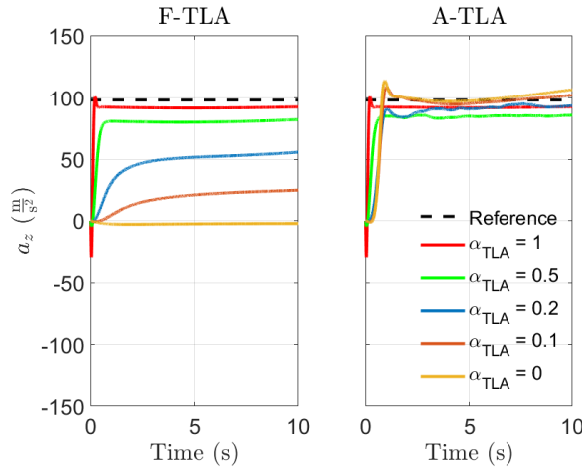


Fig. 5 The evolution of the normal acceleration for the F-TLA and A-TLA to a 10 g step command at various scalings of the gains in the TLA .

B. Harmonic Response

Next, we set $a_{z,\text{ref}} = 10g \sin(t)$. Figure 6 shows the normal acceleration tracking response with the F-TLA and the A-TLA, using the same legend and α_{TLA} scalings described previously.

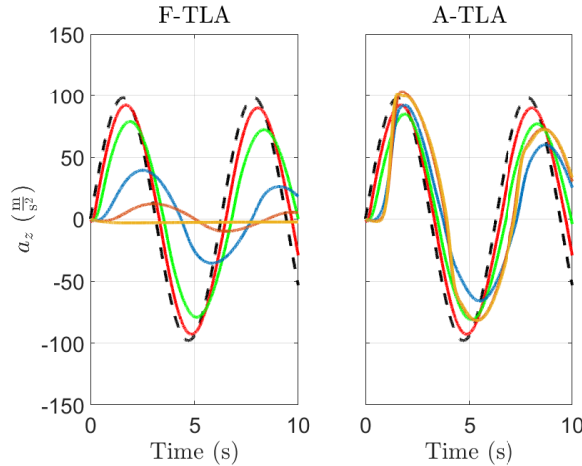


Fig. 6 The evolution of the normal acceleration for the F-TLA and A-TLA to a 10 g sinusoidal command.

C. Interception Response

Next, we consider a missile mission where the objective of the missile is to intercept a target. To achieve interception, the normal acceleration commands are generated using a proportional guidance law based on the pursuit-evasion dynamics described in Appendix B. We consider the evader model described in [17] as the target. The target's initial speed is 0.85 Mach, its flight path angle is 15 degrees, with an altitude of 4 km, and 1 km of horizontal distance from the missile.

The missile thrust is assumed to be

$$T(t) = \begin{cases} 15,000\text{N}, & t \in (0, 10), \\ 2,000\text{N}, & t \in (10, 20), \\ 0\text{N}, & t > 20. \end{cases} \quad (15)$$

The missile's initial speed is Mach 0.5, its initial flight path angle is 0 degrees, and its initial altitude is 3 km. The hyperparameters used in the RCAC are the same as those used in previous numerical simulations. Figure 7 shows the trajectory of the evader (in solid black), the trajectory of an ideal pursuer (in solid blue), the trajectory of the missile with the A-TLA (in solid green), and the trajectory of the missile with the nominally tuned F-TLA (in dashed red). Note that the ideal pursuer is assumed to be a point mass whose normal acceleration is instantaneously equal to the normal acceleration commanded by the guidance law. Furthermore, note that, in the case of a nominally tuned F-TLA, the performance of the A-TLA is similar to that of the F-TLA.

Figure 8 shows the commanded normal acceleration, the response of the missile with the F-TLA and A-TLA, and the gains of the adaptive controller updated by the RCAC algorithm. Note that, in the case of a nominally tuned F-TLA, the normal acceleration response of the A-TLA is similar to that of the F-TLA. Furthermore, note that the large increase in the normal acceleration command is due to the missile's terminal behaviour.

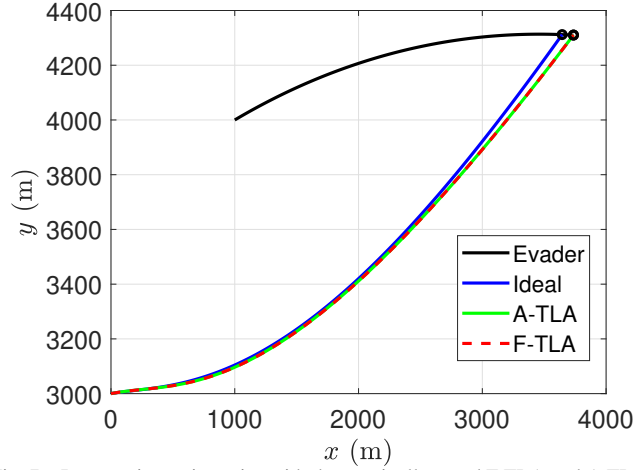


Fig. 7 Interception trajectories with the nominally tuned F-TLA and A-TLA.

Next, to investigate the performance recovery due to the adaptive augmentation, we degrade the F-TLA by scaling all of the F-TLA gains by the scalar $\alpha_{\text{TLA}} = 0.2$. Figure 9 shows the trajectory of the evader (in solid black), the trajectory of an ideal pursuer (in solid blue), the trajectory of the missile with the A-TLA (in solid green), and the trajectory of the missile with the nominally tuned F-TLA (in dashed red). Note that, in the case of off-nominal F-TLA, the interception performance degrades substantially, however, A-TLA compensates for the degraded F-TLA and recovers the performance.

Figure 10 shows the commanded normal acceleration and the response of the missile with the F-TLA and A-TLA. Note that, in the case of off-nominal F-TLA, the normal acceleration response degrades. However, A-TLA compensates for the degraded F-TLA and generates the required normal acceleration to recover performance.

Next, to investigate the robustness of the A-TLA, we vary various parameters of the nonlinear missile dynamics. In particular, we consider two scenarios, where first, we vary the fin-deflection coefficients d_N in (20) and d_M in (22), and second, we vary all the coefficients which multiply the angle of attack in (20) and (22). In each case, the coefficient to be scaled is multiplied by the scalar factor α_X . In this work, we set α_X to five equispaced values between 0.2 and 2. The interception scenario described in the previous section is considered to investigate the robustness of the the A-TLA.

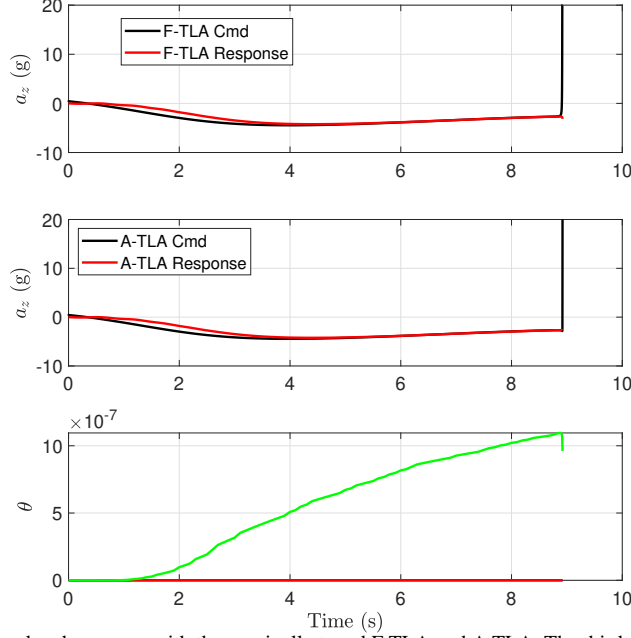


Fig. 8 Normal acceleration command and response with the nominally tuned F-TLA and A-TLA. The third subfigure shows the gains updated by RCAC.

Figure 11 shows the trajectory tracking response of the missile with the F-TLA in dashed lines and with the A-TLA in solid lines. Note that in each case, the A-TLA compensates for the variation in the missile dynamics and maintains the performance close to the ideal pursuer trajectory, whereas, the performance of the F-TLA degrades substantially in terms of time of flight and miss distance.

V. Conclusions

This paper investigated the application of a data-driven output feedback adaptive controller to improve the performance of the classical three-loop autopilot in off-nominal conditions. In particular, an adaptive proportional-integral controller, optimized by the retrospective cost adaptive control algorithm, augments a nominally tuned, fixed-gain three-loop autopilot. The particle swarm optimization framework was used to optimize the hyperparameters of the adaptive control algorithm. The particle-swarm optimized adaptive algorithm was then used to numerically investigate the performance of the adaptive three-loop autopilot in the nominal and off-nominal scenarios. Numerical simulations showed that adaptive augmentation maintains the missile's performance close to the ideal pursuer's trajectory in off-nominal scenarios, where the performance with the fixed-gain three-loop autopilot significantly degrades.

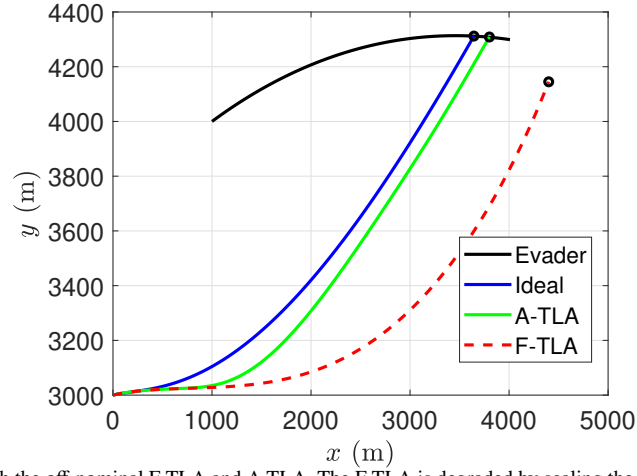


Fig. 9 Interception trajectories with the off-nominal F-TLA and A-TLA. The F-TLA is degraded by scaling the nominal fixed gains by a scalar factor $\alpha_{TLA} = 0.2$.

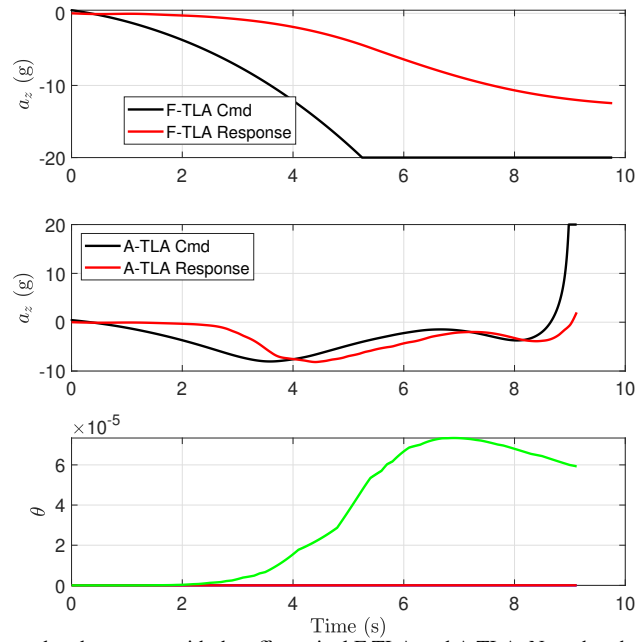


Fig. 10 Normal acceleration command and response with the off-nominal F-TLA and A-TLA. Note that the A-TLA adjusts the controller gains, shown in the third subfigure, to maintain performance.

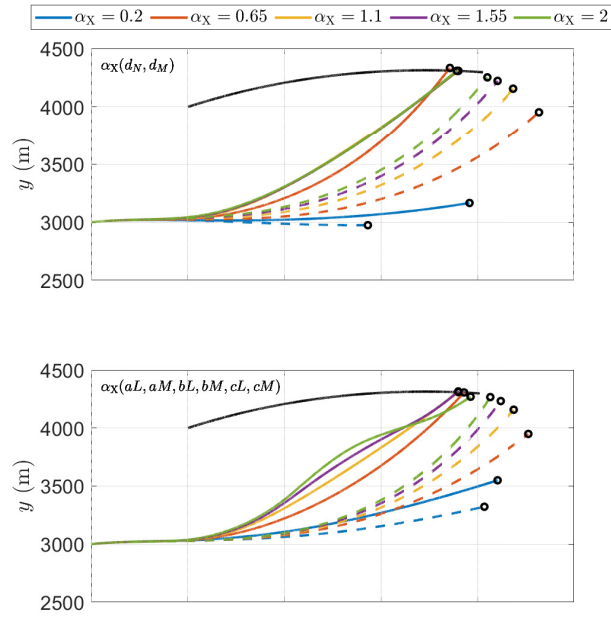


Fig. 11 Interception trajectories with the F-TLA (dashed lines) and A-TLA (solid lines) in the scenarios where a) the fin-deflection coefficient is scaled, b) the angle of attack coefficients are scaled, Note that the A-TLA maintains performance close to the ideal pursuer for a wider range of parameters.

References

- [1] Kim, S.-H., Kim, Y.-S., and Song, C., "A robust adaptive nonlinear control approach to missile autopilot design," *Control Engineering Practice*, Vol. 12, No. 2, 2004, pp. 149–154. doi:[https://doi.org/10.1016/S0967-0661\(03\)00016-9](https://doi.org/10.1016/S0967-0661(03)00016-9), URL <https://www.sciencedirect.com/science/article/pii/S0967066103000169>.
- [2] Erdos, D., Shima, T., Kharisov, E., and Hovakimyan, N., "L1 adaptive control integrated missile autopilot and guidance," *AIAA guidance, navigation, and control conference*, 2012, p. 4465.
- [3] Ouda, A. N., "A robust adaptive control approach to missile autopilot design," *International Journal of Dynamics and Control*, Vol. 6, No. 3, 2018, pp. 1239–1271. doi:10.1007/s40435-017-0352-4, URL <https://doi.org/10.1007/s40435-017-0352-4>.
- [4] Tsourdos, A., and White, B. A., "Adaptive flight control design for nonlinear missile," *Control Engineering Practice*, Vol. 13, No. 3, 2005, pp. 373–382. doi:<https://doi.org/10.1016/j.conengprac.2004.04.023>, URL <https://www.sciencedirect.com/science/article/pii/S0967066104001157>, aerospace IFAC 2002.
- [5] Lee, C.-H., Jun, B.-E., Lee, J.-I., and Tahk, M.-J., "Nonlinear missile autopilot design via three loop topology and time-delay adaptation scheme," *2013 13th International Conference on Control, Automation and Systems (ICCAS 2013)*, 2013, pp. 50–54. doi:10.1109/ICCAS.2013.6703862.
- [6] Fu, L.-C., Chang, W.-D., Yang, J.-H., and Kuo, T.-S., "Adaptive robust bank-to-turn missile autopilot design using neural networks," *Journal of Guidance, Control, and Dynamics*, Vol. 20, No. 2, 1997, pp. 346–354.
- [7] Hou, M., Liang, X., and Duan, G., "Adaptive block dynamic surface control for integrated missile guidance and autopilot," *Chinese Journal of Aeronautics*, Vol. 26, No. 3, 2013, pp. 741–750. doi:<https://doi.org/10.1016/j.cja.2013.04.035>, URL <https://www.sciencedirect.com/science/article/pii/S1000936113000861>.
- [8] Sobolic, F. M., Cruz, G., and Bernstein, D. S., "An inner-loop/outer-loop architecture for an adaptive missile autopilot," *2015 American Control Conference (ACC)*, 2015, pp. 850–855. doi:10.1109/ACC.2015.7170840.
- [9] Fuentes, R., Hoagg, J., Anderton, B., D'Amato, A., and Bernstein, D., "Investigation of cumulative retrospective cost adaptive control for missile application," *AIAA Guidance, Navigation, and Control Conference*, 2010, p. 7577.
- [10] Mracek, C., and Ridgely, D., "Missile longitudinal autopilots: connections between optimal control and classical topologies," *AIAA guidance, navigation, and control conference and exhibit*, 2005, p. 6381.
- [11] Goel, A., Islam, S. A. U., and Bernstein, D. S., "Adaptive Control of MIMO Systems Using Sparsely Parameterized Controllers," *2020 American Control Conference (ACC)*, IEEE, 2020, pp. 5340–5345.
- [12] Kamaldar, M., Islam, S. A. U., Sanjeevini, S., Goel, A., Hoagg, J. B., and Bernstein, D. S., "Adaptive digital PID control of first-order-lag-plus-dead-time dynamics with sensor, actuator, and feedback nonlinearities," *Advanced Control for Applications*, Vol. 1, No. 1, 2019, p. e20. doi:10.1002/adc2.20.
- [13] Oveissi, P., Trivedi, A., Goel, A., Tumuklu, O., Hanquist, K. M., Farahmandi, A., and Philbrick, D., "Learning-based Adaptive Thrust Regulation of Solid Fuel Ramjet," *AIAA SCITECH 2023 Forum*, 2023, p. 2533.
- [14] Oveissi, P., Goel, A., Tumuklu, O., and Hanquist, K. M., "Adaptive Combustion Regulation in Solid Fuel Ramjet," *AIAA SCITECH 2024 Forum*, 2024, p. 0743.
- [15] Rahman, Y., Xie, A., and Bernstein, D. S., "Retrospective cost adaptive control: Pole placement, frequency response, and connections with LQG control," *IEEE Control Systems Magazine*, Vol. 37, No. 5, 2017, pp. 28–69.
- [16] Goel, A., U. Islam, S. A., and Bernstein, D. S., "Adaptive Control of MIMO Systems Using Sparsely Parameterized Controllers," *2020 American Control Conference (ACC)*, 2020, pp. 5340–5345. doi:10.23919/ACC45564.2020.9147513.
- [17] Islam, S. A. U., and Bernstein, D., "Minimum Time-of-Flight Interceptor Guidance Using Real-Time-Implementable Model-Predictive Guidance," *AIAA SCITECH 2022 Forum*, 2022, p. 1377.
- [18] Kabamba, P. T., and Girard, A. R., *Fundamentals of Aerospace navigation and guidance*, Cambridge University Press, 2014.

Appendix A: Missile Longitudinal Dynamics

As shown in Figure 1, $\vec{v}_{c/w/A} = V\hat{i}_C$, and thus

$$\vec{a}_{c/w/A} = \dot{V}\hat{i}_C + V\dot{\hat{i}}_C = \dot{V}\hat{i}_C - V\dot{\gamma}\hat{k}_C. \quad (16)$$

The total force on the missile is

$$\begin{aligned} \vec{f}_B &= mg\hat{k}_A - f_n\hat{k}_B - f_a\hat{i}_B + T\hat{i}_B \\ &= (-mg\sin(\gamma) - f_n\sin(\alpha) + (T - f_a)\cos(\alpha))\hat{i}_C + (mg\cos(\gamma) - f_n\cos(\alpha) - (T - f_a)\sin(\alpha))\hat{k}_C, \end{aligned} \quad (17)$$

where m is the mass of the missile, g is the acceleration due to gravity, f_n and f_a are the normal and axial aerodynamic forces on the missile, and T is the thrust, and the total moment relative to c is

$$\vec{M}_{B/c} = \mathcal{M}\hat{j}_B, \quad (18)$$

where the aerodynamic forces and moments are parameterized by

$$f_n = \frac{1}{2}\rho SV^2 C_N, \quad f_a = \frac{1}{2}\rho SV^2 C_A, \quad \mathcal{M} = \frac{1}{2}\rho SV^2 d C_M, \quad (19)$$

where d is the chord length, S is the reference surface area, and ρ is the air density calculated by the International Standard Atmosphere model. Furthermore, the aerodynamic coefficients C_N , C_A , and C_M are parameterized by

$$C_N = a_N\alpha^3 + b_N\alpha|\alpha| + c_N(2 - M/3)\alpha + d_N\delta, \quad (20)$$

$$C_A = a_A, \quad (21)$$

$$C_M = a_M\alpha^3 + b_M\alpha|\alpha| + c_M(8M/3 - 7)\alpha + d_M\delta + e_Mq, \quad (22)$$

where δ is the fin deflection angle. The transfer function from the fin deflection angle command u to the fin deflection angle δ is

$$G_{\delta u}(s) = \frac{\omega_a^2}{s^2 + 2\zeta\omega_a + \omega_a^2}. \quad (23)$$

where ζ is the damping ratio and ω_a is the natural frequency of the actuator.

Resolving the force \vec{f}_B and the inertial acceleration $\vec{v}_{c/w/A}^{\bullet}$ in F_C , and using the Newton's second law, $m\vec{v}_{c/w/A}^{\bullet} = \vec{f}_B$, yields

$$m\dot{V} = -mg\sin(\gamma) - f_n\sin(\alpha) + (T - f_a)\cos(\alpha), \quad (24)$$

$$-mV\dot{\gamma} = mg\cos(\gamma) - f_n\cos(\alpha) - (T - f_a)\sin(\alpha). \quad (25)$$

Similarly, resolving the moment $\vec{M}_{B/c}$ in F_C and using the Euler's equation yields

$$I_y\ddot{\theta} = \mathcal{M}. \quad (26)$$

which can be rewritten in the state-space form as

$$\dot{\theta} = q, \quad \dot{q} = \frac{\rho V^2 S d}{2I_y} C_M, \quad (27)$$

where q is the pitch rate.

For the simulations presented in this work, the values of the parameters parameterizing the aerodynamic coefficient are given in Table 1, and the physical properties of the missile are given in Table 2.

Parameter	Value	Parameter	Value
a_N	-19.373	a_M	40.440
b_N	31.023	b_M	-64.015
c_N	9.717	c_M	2.922
d_N	1.948	d_M	-11.803
a_A	0.3005	e_m	-1.719
ω_a	150 rad/s	ζ	0.7

Table 1 Parameter values.

Parameter	Value	Parameter	Value
Mass m	204.0227 kg	S	0.0409 m ²
d	0.2286 m	I_y	247.4336 kg m ²
d_{imu}	0.5 m		

Table 2 Physical properties of the missile.

Appendix B: Interception Guidance

This appendix describes the derivation of the normal acceleration command using proportional guidance. A planar interception geometry for a pursuer P and an evader E is shown in Figure 12 [18]. The interception dynamics for the

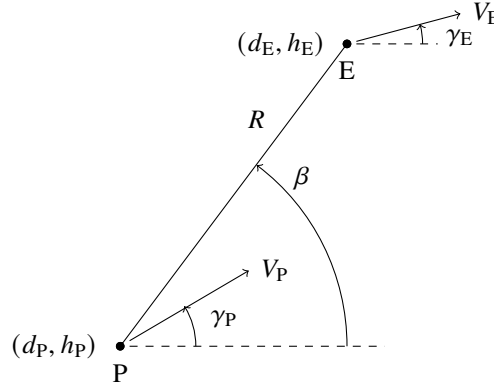


Fig. 12 Interception geometry for the pursuer and the evader.

pursuer and the evader is

$$\dot{V}_P = \frac{T_P - D_P}{m_P} - g \sin \gamma_P, \quad (28)$$

$$\dot{V}_E = \frac{T_E - D_E}{m_E} - g \sin \gamma_E, \quad (29)$$

$$\dot{\gamma}_P = -\frac{1}{V_P} \left(\frac{T_{z,P}}{m_P} + g \cos \gamma_P \right), \quad (30)$$

$$\dot{\gamma}_E = -\frac{1}{V_E} (n_{z,E} + g \cos \gamma_E), \quad (31)$$

where V_P, V_E are the velocities, γ_P, γ_E are the flight-path angles, T_P, T_E are the thrust, D_P, D_E are the drag, and $n_{z,P}, n_{z,E}$ are the normal accelerations of the pursuer and evader, respectively. The line of sight angle β satisfies

$$\dot{\beta} = \frac{1}{R} (V_P \sin(\beta - \gamma_P) - V_E \sin(\beta - \gamma_E)) \quad (32)$$

The proportional guidance law is

$$\dot{\gamma}_P = \lambda \dot{\beta}. \quad (33)$$

Substituting (30) and (32) in (33) yields the normal acceleration command

$$n_{z,P} = -\frac{V_P}{R} (V_P \sin(\beta - \gamma_P) - V_E \sin(\beta - \gamma_E)) - g \cos \gamma_P. \quad (34)$$